Applied Surface Science 391 (2017) 548–556

Contents lists available at ScienceDirect

Applied Surface Science

journal homepage: www.elsevier.com/locate/apsusc

Effect of reaction parameters on photoluminescence and photocatalytic activity of zinc sulfide nanosphere synthesized by hydrothermal route

T. Inakhunbi Chanu [a], Dhrubajyoti Samanta [a], Archana Tiwari [b], Somenath Chatterjee [a,c,*]

[a] Centre for Material Science and Nanotechnology, Sikkim Manipal Institute of Technology, Sikkim Manipal University, Sikkim 737136, India
[b] Department of Physics, Sikkim University, 737102 Sikkim, India
[c] Electronics & Communication Engineering Department, Sikkim Manipal Institute of Technology, Sikkim Manipal University, Sikkim 737136, India

ARTICLE INFO

Article history:
Received 2 February 2016
Received in revised form 7 May 2016
Accepted 9 May 2016
Available online 11 May 2016

Keywords:
Hydrothermal synthesis
ZnS nanosphere
Photoluminescence
Degradation mechanism of RhB
Photocatalysis

ABSTRACT

Zinc Sulfide (ZnS) nanospheres have been synthesized using amino acid, L-Histidine as a capping agent by hydrothermal method. The as prepared ZnS have been characterised using X-ray Diffraction (XRD), Field Emission Scanning Electron Microscopy (FESEM), High Resolution Transmission Electron Microscopy (HRTEM), Photoluminescence (PL), Fourier Transform Infra-Red spectroscopy (FTIR), UV–vis absorption spectroscopy and X-ray Photo Electron Spectroscopy (XPS). Effect of reaction parameters on particle size has been investigated. The morphology and size of the ZnS can be tuned based on the reaction parameters. ZnS nanosphere with a particle size of 5 nm is obtained when the reaction parameters are kept at 120 °C for 3 h. The PL of ZnS shows multiple defect emissions arising from interstitials/vacancies. Particle size of ZnS nanoparticles plays an important role in determining the photo catalytic activity. A chronological study on synthesis of ZnS nanosphere and its photo catalytic activity under the sunlight are discussed here, which reveals the photo degradation of Rhodamine B (RhB) upto 87% as observed with ZnS nanosphere having a particle size of 5 nm.

1. Introduction

Significant interest on Zinc based semiconductor nanomaterials, e.g. ZnO, ZnS etc. in the research is due to its credibility as a material with excellent possibilities [1–3]. ZnS belongs to II–VI group of semiconductor having direct band gap energy of 3·68 eV at room temperature and exhibit large exciton binding energy of 40 meV [4]. ZnS shows wide applications ranging from sensors, photo catalysts and biomedical fields [5–7]. The tunability of optical and chemical properties for nanomaterials depends on the size, shape and crytallinity of the particles. Zero-dimensional (0D) ZnS nanostructures have been used for biological detection and tagging [8]. One dimensional (1D) ZnS, such as nanobelts and nanowires, have shown their promising applications in the optoelectronics and LASERarea [9,10]. Depending on the various synthetic method, different size of nanoparticles of ZnS may be obtained. Several methods have been reported on synthesis of ZnS nanoparticles such as co-precipitation, chemical vapor deposition, hydrothermal method [11–13] etc. Hydrothermal method is one of the simple synthetic route to tune the desire size and morphology of the particles, which may be acquired by changing parameters such as reaction precursors, temperature and time during growth process [14,15]. The capping agents have been used in the synthesis of nanomaterials to control the agglomeration, stability, shape and size of the same. Mostly, polymers and biomolecules have been used as a capping agent in the synthesis of various semiconductor nanomaterials [16,17]. Among the biomolecules, amino acids have successfully been used as capping agents [18–20] and depending on the pH, these molecules exist in different ionic form which influence the bonding with the metal ion precursors. This in turn tune shape, size and physical properties of the semiconductor nanomaterials. L-Histidine assisted ZnS microspheres and glycine assisted TiO_2 microflower have been reported and their photo catalytic activity have been studied [20,21]. PL is one of the most sensitive technique and nature of the nanomaterial can be determined from the PL spectra. The tuning of lumisecence properties of ZnS can be achieved by doping with metals. For example, blue, green and orange emission have been observed with the dopant candidates, e.g. Mg, Cu and

* Corresponding author: Electronics & Communication Engineering Department, and Centre for Material Science and Nanotechnology, Sikkim Manipal Institute of Technology, Sikkim Manipal University, Sikkim, India.
E-mail address: somenath@gmail.com (S. Chatterjee).

http://dx.doi.org/10.1016/j.apsusc.2016.05.045
0169-4332/

Mn in ZnS nanoparticles, respectively [22–24]. The optical properties of ZnS are also sensitive to size, shape, and crystal structure [25,26]. ZnS in the form of nanowires, nanobelts and nanoribbons have shown near-UV emission band as well as green emission centred at around 520 nm [27–29]. The optical properties of ZnS can also be tuned depending on the presence of different defect states arising from sulphur and zinc related defects [30,31]. Studies the nature of the PL is important to determine the structure of the nanomaterials. Here, we report the multiple PL emission arising from the different defect states of ZnS synthesized by hydrothermal method using L-Histidine as capping agent. This current finding may help to obtain the desire PL just by changing the growth parameters. ZnS has shown high photo catalytic activity for the photo catalytic degradation of several organic pollutants and photo catalytic splitting of water for production of H_2 [32–41]. Due to wide band gap (3.68 eV) nature of ZnS, its photo response activity is restricted in the UV region of solar radiation. Extensive work on the photo catalytic activity of ZnS have been reported under the exposure of suitable light source. However, utilization of direct sunlight as a light source for UV region is limited as only 4% solar radiation is occupied in UV region. Therefore there is still need to be explored on the synthesis of nanomaterial which can utilize the natural sunlight. Herein, the photo catalytic activity of the ZnS has been studied by utilizing natural sunlight as light source. Rhodamine B (RhB) dye has been used as model to demonstrate the photo catalytic activity of ZnS through photo degradation mechanism under sunlight illumination. Most of recent experimental findings have revealed that the sizes of L-Histidine assisted ZnS materials in hydrothermal synthesis are in microsphere range. However, in the present study, ZnS nanomaterial with 5 nm average size was obtained following the modified synthesis process using the same capping agent.

2. Experimental details

2.1. Chemicals

All the chemicals were of analytical grade and used without further purifications. Zinc nitrate hexahydrate ($Zn(NO_3)_2{\cdot}6H_2O$), Rhodamine B (RhB) and Sodium hydroxide (NaOH) were purchased from Loba Chemie. Sodium Sulphide ($Na_2S{\cdot}9H_2O$) was purchased from Rankem. L-Histidine ($C_6H_9N_3O_2$) was procured from Hi Media. De ionized (DI) water (resistivity: 18.5 MΩ-cm) was used for all analysis.

2.2. Instrumentation

Structural characterization of samples were done using X-ray powder diffraction measurements recorded using X-ray diffractometer (PAN Alytical Spectristechnologies PW 3040/60). UV–vis absorption spectra of all the samples were performed using shimadzu 1800 UV–vis spectrophotometer. PL measurements were executed using a perkin-Elmer LS55 fluorescence spectrometer. The FTIR of the samples were done using perkin-Elmer FTIR spectrometer. The XPS analysis was carried out using Omicron Nanotechnology instrument. The morphology and composition of the samples were verified using Zeiss Auriga compact field emission scanning electron microscope (FESEM) equipped with an energy dispersive X-ray analyser (EDX). FEI TECHNAI G2 high resolution transmission electron microscope (HRTEM) was used for the identification of crystallinity size, selected area electron diffraction (SAED) and lattice fringes of the samples.

2.3. Methodology

Zn $(NO_3)_2{\cdot}6H_2O$ and L-Histidine were dissolved in DI water and stirred at room temperature for 30 min. Then Na_2S solution was added into the same slowly while stirring. The molar ratio of L-Histidine, zinc and sulphur sources were maintained at 1:1:1. The solution was transferred to the 250 ml Teflon-lined stainless steel autoclave system and maintained the final volume at 100 ml. Then the autoclave was placed inside the preheated muffle furnace at temperature 120 °C for 3 h and then cooled down to room temperature naturally. The solution containing products were centrifuged, washed several times with DI water and methanol to remove the impurities. Finally the sample was dried at 80 °C for 3 h. To prepare other samples, the synthesis processes were same; however, the reaction duration and temperature were varied. The details of sample parameters are given in Table 1.

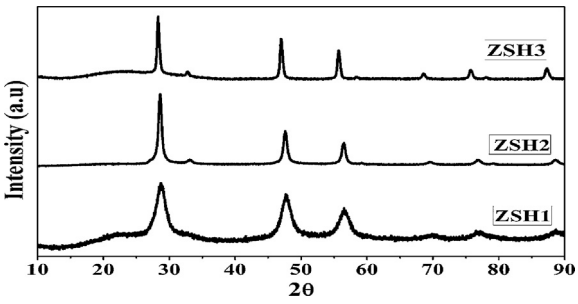

Fig. 1. X-ray diffraction patterns of ZnS nanosphere prepared at 120 °C for different reaction time.

To study the absorption characteristics and PL measurement, equal amount of contents for each samples were dissolved in 3.5 ml DI water and ultra-sonicated for 20 min for dispersion. For the photo catalytic studies, to a 5 ml of RhB (5 μM) solution, 5 mg of as-synthesized ZnS was mixed together and was shaken for 30 min using water bath shaker. The reaction mixture was kept in dark for 1 h to attain equilibrium. Then the reaction mixture were exposed to sun-light for different interval of duration with intermittent shaking for uniform mixing of the photo catalysts with the RhB solution. After the sunlight exposure at regular interval, the photo catalysts were removed by centrifugation. The supernatant solution containing RhB concentration was monitored by UV–vis absorption spectroscopy at 554 nm with DI water as the reference medium. The degradation efficiency of the photo catalysts was calculated using the following formula:

$$DegradationEfficiency = \frac{C_0 - C_t}{C_0} \times 100 \quad (1)$$

where C_0 and C_t are the initial and time dependent concentrations of RhB.

3. Results and discussion

3.1. Structural and morphology characterisation

Fig. 1 shows the XRD patterns of the ZnS prepared at 120 °C for different reaction time for samples denoted as ZSH1, ZSH2 and ZSH3 (corresponding specifications are mentioned in Table 1). The diffraction peaks at 2θ (in degree) values are observed at 28.6°, 33.1°, 47.6° and 56.4°, which corresponds to (111), (200), (220) and (311) planes, respectively of the zinc blende cubic structure for ZnS (according to JCPDS Card No. 05-0566). No diffraction peaks from other crystalline phases are observed, indicating the high purity and crystallinity of ZnS. It can also be seen that the peaks are relatively broad, suggesting the existence of smaller particle size. The average crystallite sizes in the ZnS are estimated using the following Debye Scherrer equation:

$$D = \frac{k\lambda}{\beta Cos\theta} \quad (2)$$

Table 1
Notations of the hydrothermally synthesized ZnS.

Sl No	Notations	Reaction Parameters			Precursor Ratio			Calcination Temperature (°C)	Particle Size From XRD (nm)
		Time (h)	Temperature (°C)	pH	Zn^{2+}	S^{2-}	L-Histidine		
1	ZSH1	3	120	5	1	1	1	–	4.2
2	ZSH2	5	120	5	1	1	1	–	12.9
3	ZSH3	8	120	5	1	1	1	–	18.5
4	ZSH4	5	80	5	1	1	1	–	11.0
5	ZSH5	5	150	5	1	1	1	–	26.6
6	ZSH6	5	180	5	1	1	1	–	47.8
7	ZSH7	3	120	10.5	1	1	1	–	18.0
8	ZSH8	3	120	5	1	1	2	–	23.0
9	ZSH9	3	120	5	1	1	1	300	27.0

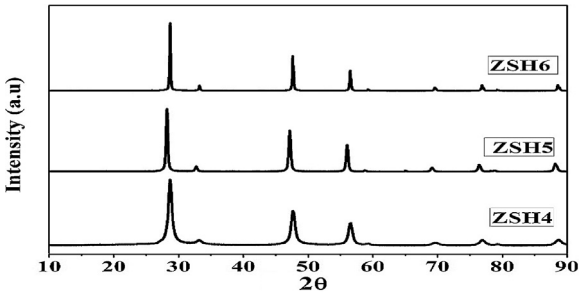

Fig. 2. X-ray diffraction patterns of ZnS nanosphere prepared at 5 h for different temperature.

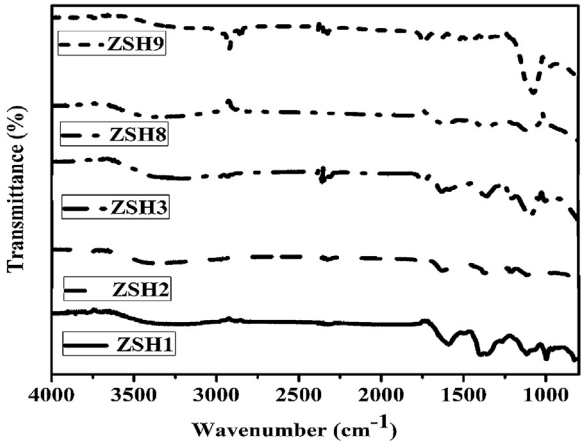

Fig. 3. FTIR spectra of ZnS samples with different reaction parameters.

where k = 0.9 is the shape factor, λ is the incident X-ray wavelength of Cu Kα radiation (1.5408 Å), θ is the Bragg diffraction angle, and β is the full width at half maximum (FWHM) of the (111) plane. The particle sizes of ZnS are calculated to be 4.2 nm, 12.9 nm and 18.5 nm for ZSH1, ZSH2 and ZSH3, respectively, suggesting the increase in particle size with increment in reaction time. It has been reported that in hydrothermal synthetic route, the size of particle can be tuned by varying the reaction parameters, e.g. temperature and time [15]. We have also investigated the effect of temperature on the particle size for ZnS, as shown in Fig. 2. The particle sizes are calculated to be 11 nm, 26.6 nm and 47.8 nm for ZSH4, ZSH5 and ZSH6 samples, respectively. It can also be seen from XRD (shown in supplementary information S1) of the ZnS samples denoted as ZSH7 and ZSH8, ZSH9 that the particle size are calculated to be 18 nm and 23 nm and 27 nm, respectively, suggesting the increase in particle size while keeping the same reaction temperature and time. For ZSH7 sample, the starting pH was kept at 10.5 while keeping reaction condition at 120 °C for 3 h with precursor ratio 1:1:1. For ZSH8 sample, the concentration of L-Histidine was increased to two fold while keeping reaction condition at 120 °C for 3 h and starting pH = 5. The ZSH9 denotes the calcined sample at 300 °C. This indicates that in addition to reaction temperature and time; starting pH, concentration of the precursor and calcination, also affect the particle size of the ZnS.

To determine the presence of L-Histidine on ZnS, FTIR spectra of ZnS samples are recorded, which is shown in Fig. 3. In all samples, the broad band around 3500 cm^{-1} and a sharp band at 1600 cm^{-1} can be observed. Devi et al. [42] recorded the FTIR spectrum of L-Histidine stabilized colloidal ZnS nanoparticles to determine the presence of L-Histidine over ZnS. The broad band in the region of 3200–3600 cm^{-1} and 1600 cm^{-1} were assigned to the N—H stretching vibrations of the amino group and the vibrations of the >COO group of Histidine. Therefore the band observed at 3600 cm^{-1} and 1600 cm^{-1} can be attributed from the L-Histidine which is present on the surface of the ZnS nanoparticles. The IR spectra of the remaining ZnS samples are shown in Supplementary information S2. The presence of L-Histidine is further confirmed from the EDX pattern which is shown in supplementary information S3 that in addition to the Zn and S peaks, there is also presence of peaks corresponding to C, N and O of L-Histidine composition.

The size and morphology of ZnS can be obtained from HRTEM image. Fig. 4 shows the HRTEM image of the ZSH1 sample. The particles are well dispersed with particle shape in the form of nanosphere distributed uniformly at 50 nm scale (as shown in Fig. 4a). The particles sizes are in the range of 2 nm to 8 nm with a very few number at 12 nm and 18 nm. From the histogram of the image (Fig. 4b), the average particle size is calculated to be 5 nm which supports the results obtained from XRD analysis for the same sample. As observed from the lattice fringes of the image (Fig. 4c), the inter-planner spacing (d_{hkl}) is calculated to be 2.7 Å, corresponding to the (200) plane. The selected area electron diffraction (SAED) pattern of ZnS nanosphere is shown in Fig. 4d. The SAED pattern shows a set of rings instead of spots indicating that ZnS nanosphere are polycrystalline in nature and resemble to (200) plane, which confirms the XRD obtained results.

The HRTEM image for the ZSH3 is shown in Fig. 5a. Different sizes and shapes of the particles are found for the ZSH3 sample, whereas a uniform shape and sizes are observed for ZSH1 sample and the particle size is larger compared to ZSH1, which infers the time-dependency of the synthesis process. Also the particles are found to be agglomerated with the formation of multilayers and various particle size ranging from 10 nm to 100 nm and a very few up to 150 nm as can be seen from histogram (Fig. 5b). The average particle size is calculated to be 50 nm, which is much bigger than the one calculated from the XRD, which suggest that the obtained products are polycrystalline in nature. Fig. 5c shows the presence of lattice fringes with d_{hkl} spacing of 3.1 Å which correspond to the (111) plane as confirmed from XRD. The polycrystalline nature of the material is confirmed from SAED pattern (Fig. 5d) with assigning some of plane to (111) and (220) plane.

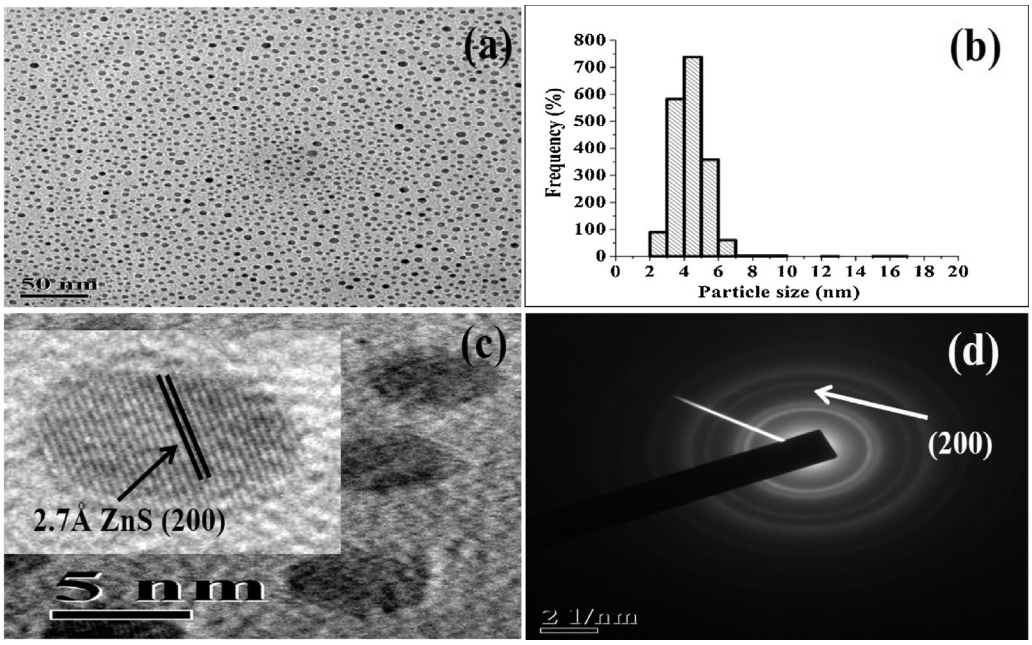

Fig. 4. (a) TEM image, (b) histogram, (c) HR TEM image showing lattice fringes and (d) SAED pattern for ZSH1, respectively.

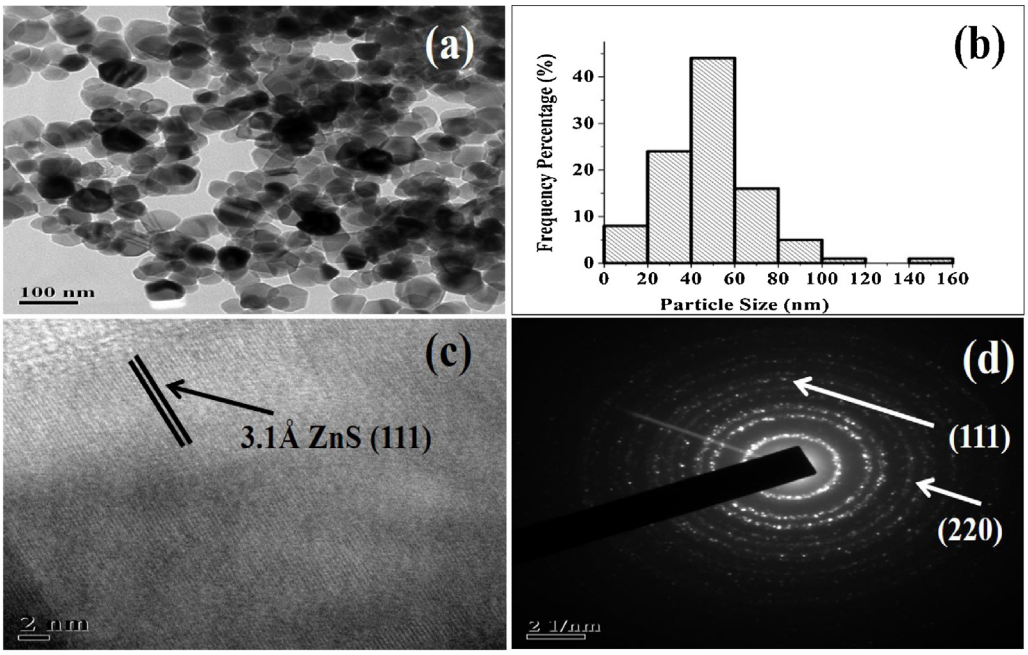

Fig. 5. (a) TEM Image, (b) histogram, (c) HR TEM image showing lattice fringes and (d) SAED pattern for ZSH3 sample, respectively.

3.2. XPS analysis

To determine the chemical composition of the prepared ZnS samples, XPS analysis is carried out. Fig. 6 shows the XPS analysis of ZSH1 sample. The scan survey (Fig. 6a) shows the presence of Zn 2p, S 2s, S 2p, C 1s and O1s peaks. The appearance of O1s and C1s peaks at 527 eV and 264 eV could be attributed to the presence of L-Hisitidine. In Fig. 6b, the binding energy observed at 1045 eV and 1021 eV corresponds to Zn $2p_{1/2}$ and Zn $2p_{3/2}$ respectively. And from Fig. 6c binding energy observed at 162 eV correspond to S $2p_{1/2}$. These values are in accordance with the reported work of ZnS [43–45]. It can also be seen that there is an absence of peak at 168 eV due to sulfate related peak, which indicate that the ZnS is resistant to photocorrosive oxidation and exhibit high stability in air [44].

3.3. Optical properties

The UV–vis absorption spectra of ZnS prepared at 120 °C with different reaction time are shown in Fig. 7a. It can be seen from the absorption spectra that the shoulder peak of each spectrum is blue shifted compared to bulk ZnS. The optical band gap energy is calculated from the Tauc relation [46,47], which is given by the following equation:

$$\alpha h\nu = B(h\nu - E_g)^{\frac{1}{2}} \quad (3)$$

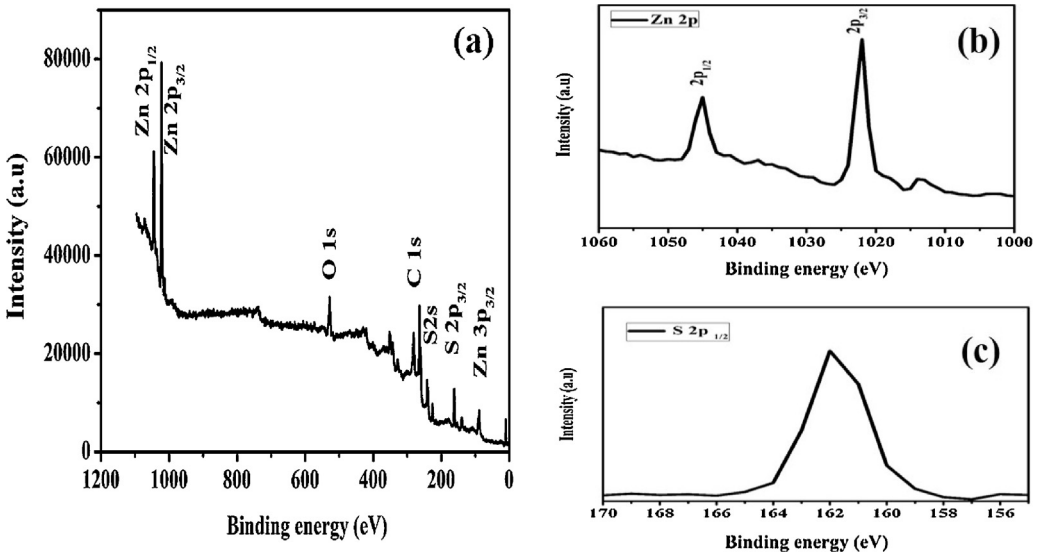

Fig. 6. (a) Scan survey of XPS spectrum of ZSH1 sample (b) Zn 2p spectrum and (c) S 2p spectrum.

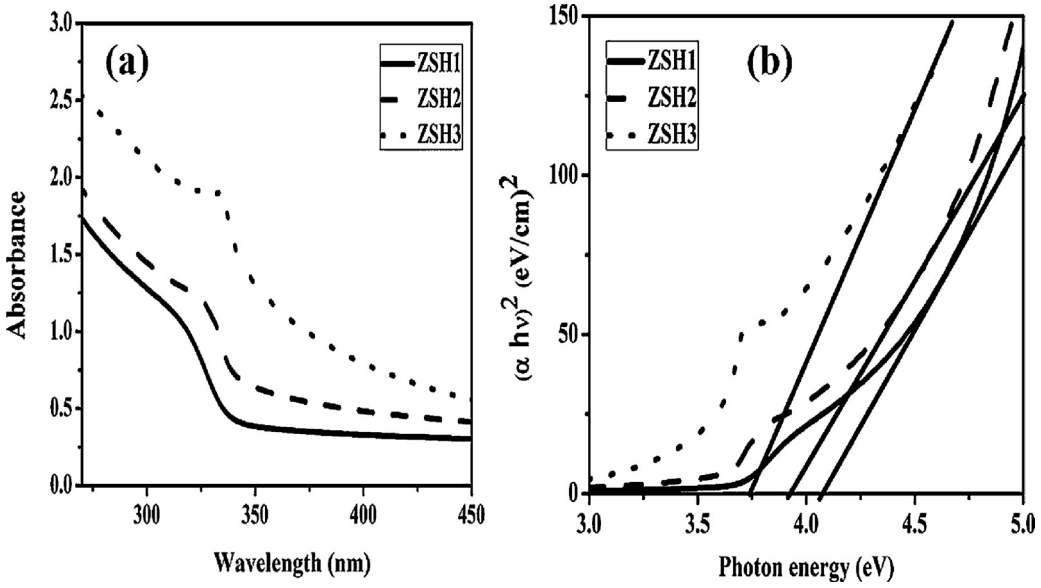

Fig. 7. (a) UV–vis absorption spectra and (b) tauc plot of the ZnS samples of ZSH1, ZSH2 and ZSH3, respectively.

where α is the absorption co-effiecient, hυ is the photon energy, E_g is the direct band gap, and B is a constant. The band gap energy is calculated from the plot of $(\alpha h\upsilon)^2$ versus hυ, which is shown in Fig. 7b. The extrapolating the linear portion of the curve to the energy axis yields the band gap energy. The estimated band gap energy of the samples are calculated to be 4.07 eV, 3.94 eV, 3.76 eV for the samples ZSH1, ZSH2 and ZSH3, respectively. The band gap energy of the bulk ZnS is 3.67 eV [4]. The blue shift in band gap energy is attributed to the quantum size effect, which supports the HRTEM observations for the same samples.

In order to determine the emission behaviour of the synthesized ZnS, room temperature PL spectra were recorded by exciting the samples with excitation wavelength of 300 nm and measured the PL spectra from 320 nm to 580 nm. The baseline correction was done for all PL spectra. The effect of reaction time on PL of ZnS is shown in Fig. 8a. It can be seen that there are multiple emission peaks observed at 363 nm, 423 nm, 443 nm, 486 nm and 531 nm, respectively. The 363 nm peak is broad attributing to the presence of more than one peak in its envelop. This indicates that in addition to band edge emission, the possibility of existence for many defect states in ZnS. Since the particle is polycrystalline in nature as confirmed from SAED pattern, there could be the presence of many defect states arising from sulphur and zinc related defects. Wang et al. [48] reported the multiple defect related emission of ZnS. It can be observed that emissions intensity are found to be decreased on increasing the reaction time. The increase in the reaction temperature also shows a reduction in the emission intensity, which is shown in Fig. 8b. The emission intensity is drastically decreased in ZSH6. The decrease in emission intensity might be due to the increase in particle size as shown in Table 1. The particle size is found to be as small as 5 nm in the case of ZSH1 and it shows maximum emission intensity. As the particle size increases, the emission intensities are found to be decreased. It was reported that the smaller the particle size produces larger surface area and the larger surface area caused the stronger photoluminescence intensity [49]. Therefore, the decrease in the emission intensities with respect to increase in particle size can be attributed to the decrease in the surface area.

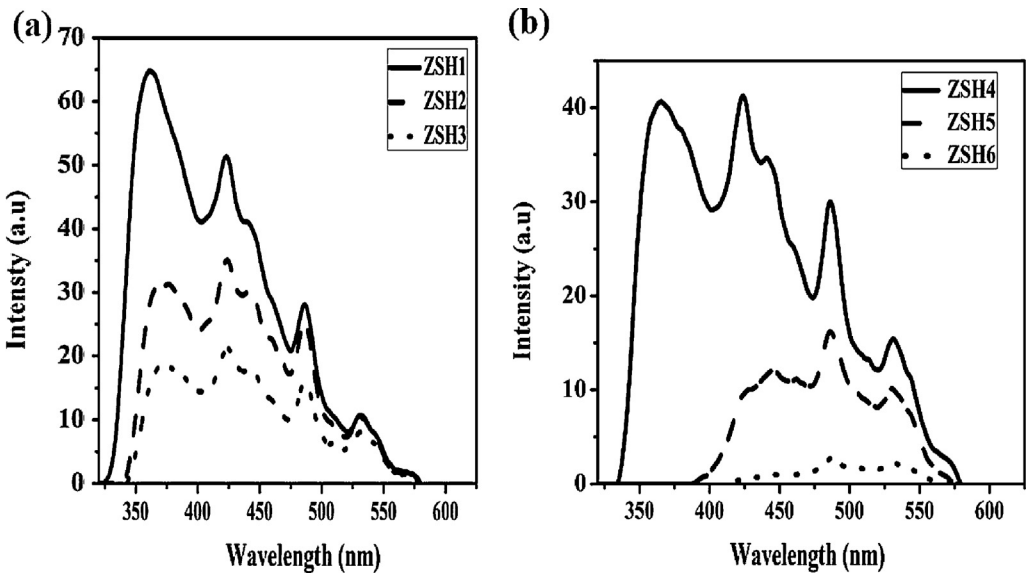

Fig. 8. Photoluminescence spectra of ZnS samples (a) Effect of reaction time (ZSH1, ZSH2 and ZSH3) and (b) effect of reaction temperature (ZSH4, ZSH5 and ZSH6).

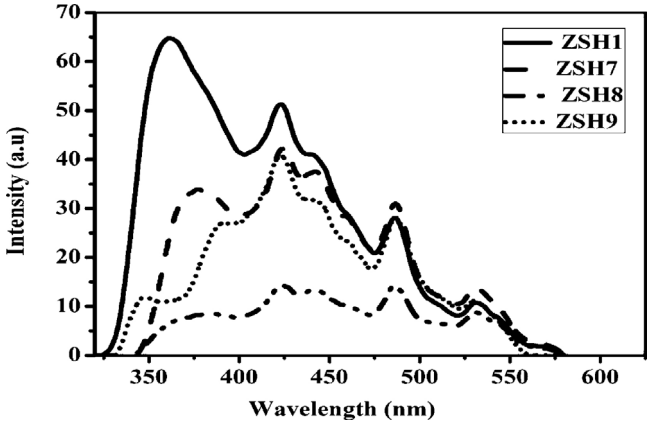

Fig. 9. Effect of reaction parameters on Photoluminescence spectra of ZnS for samples ZSH1 (reaction time), ZSH7 (starting pH), ZSH8 (precursor ratio) and ZSH9 (calcined sample), respectively.

In addition to reaction parameters such as temperature and time, the effect on the PL spectra of ZnS by other parameters such as starting pH, precursor ratio and calcinations are also investigated. Fig. 9 shows the PL spectra of ZnS sample denoted as ZSH7, ZSH8 and ZSH9. It can be seen that the emission intensity at 363 nm is observed to be reduced for ZSH7 which is prepared at starting pH of 10.5. However the defect emission observed at 486 nm and 530 nm are found to be slightly increased with increasing in pH. It infers that with increase in pH there is a decreased in band edge emission, however defect emission increases. This attributes that with the higher pH, there might be more formation of defect related states on the surface of the particles. It can also be observed from Fig. 9 that, emission spectra is reduced for ZSH8 sample. The concentration of L-Histidine is kept two times higher in ZSH8 sample. Whereas, for ZSH9 sample which is calcined sample, there is an absence of peak at 363 nm and two peaks are observed at 345 nm and 390 nm, respectively, associated with many defect peaks. The pKa values of L-Histidine is reported to be 1.8, 6.0 and 9.2 for carboxyl, imidazole and amino group of L-Histidine [50]. This indicates that at pH below 6, only carboxyl group is deprotonated. At pH 7, both carboxyl and imidazole group are deprotonated. And at pH 10.5, all the binding sites including amino group of L-Histidine are deprotonated. This suggest that at pH 10.5, there are possibility of formation a stable complex between L-Histidine and Zn^{2+} ion through all three binding sites of L-Histidine. Devi et al. [42] reported the enhancement of the PL intensity due to L-Histidine stabilized colloidal ZnS prepared with increasing pH. They explained that at high pH, there is a presence of more binding site between L-Histidine and Zn^{2+} ion to form a stable complex. However in our present case, due to the high temperature and pressure condition during synthesis as well as more binding sites due to increasing pH, influence the formation of more electrostatic effect [21,51], which could lead the aggregation of the particles and thus increases the particle size. The presence of excess amount of L-Histidine might not only increases the particle size but also saturated the surface state. The emission peak at 363 nm is actually consists of two peaks with emission at 345 nm and 390 nm which clearly separate for the sample calcined at 300 °C. Therefore, 345 nm can be assigned to band edge emission. And the emission at 390 nm, 423 nm, 443 nm, 486 and 530 nm are associated with the defect state emission arising from sulphur and zinc defect state. It has been reported that interstitial sulphur states and zinc vacancies states are located closer to valence band and act as acceptor state, whereas as interstitial zinc states and sulphur vacancies state are located near to the conduction band edge and act as localized donor state [52]. Accordingly, the emission behaviour can be assigned to the respective defect states. The emission at 423 nm can be attributed to the recombination of electrons at the internal sulphur vacancy (I_s) donor level with holes trapped at the internal zinc vacancy (V_{Zn}) acceptor level [30,53]. The blue emission peak observed at 445 nm could be associated with an interstitial zinc (I_{zn}) lattice defect and the emission peak at 486 nm is from the sulphur vacancy (V_s) related emission [53]. The green PL emission peak at 530 nm can be associated with elemental S species [49,54].

3.4. Photocatalytic studies

The potential of the photocatalytic activity of ZnS has been investigated by observing the photo degradation of RhB dye in aqueous media using sunlight as a light source. The concentration of RhB was kept at 5 μM. The experiment was carried out when the intensity of sunlight is maximum between 11:30 AM to 2 PM having light intensity of 1040 × 100 lx. To avoid the different intensity of sunlight, all the experiment were carried out on same day and placed the samples in such a way that light falls uniformly on

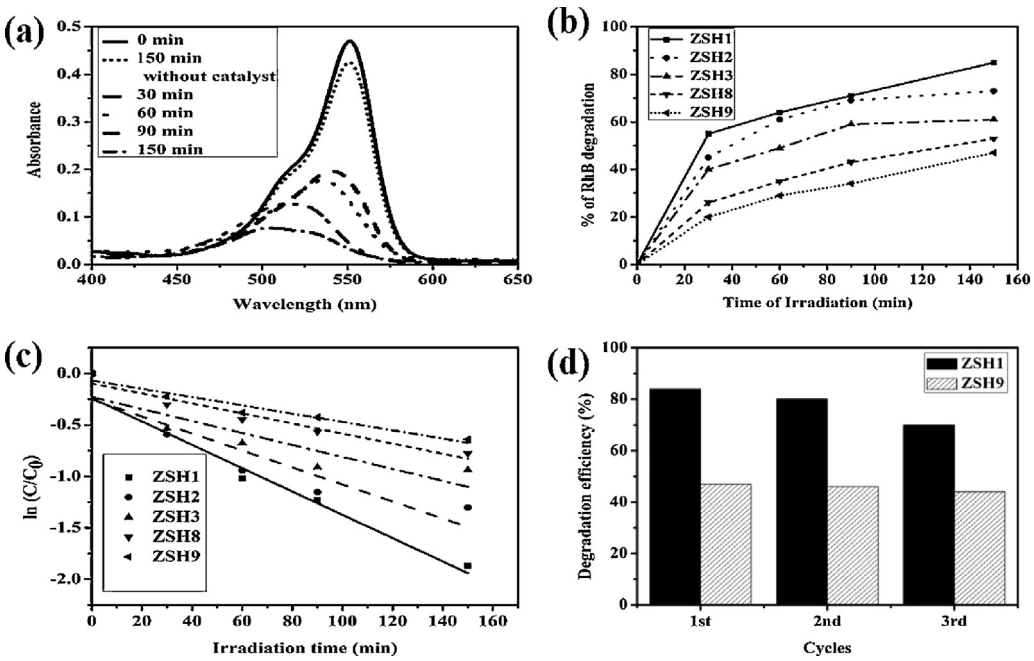

Fig. 10. (a) Absorption spectra showing the photocatalytic degradation of RhB with catalyst ZSH1 under sunlight (b) percentage of RhB degradation (c) kinetic plot of ln C/C_0 versus irradiation time and (d) reusability test of catalyst ZSH1 and ZSH9 respectively for degradation of RhB.

Table 2
Photodegradation data of RhB in the presence of ZnS samples.

Notation	Degradation efficiency (%)	Rate constant k (min^{-1})
ZSH1	87	0.0113
ZSH2	73	0.0083
ZSH3	61	0.0058
ZSH8	53	0.0049
ZSH9	47	0.0041

all samples. The UV visible absorption spectra for the degradation of the dye as a function of irradiation time are shown in Fig. 10(a) with ZSH1. The absorption peak of the dye at 554 nm is found to be decreased as well as blue shifted on increasing the irradiation time, suggesting the increase in degradation as the time of irradiation by solar energy. It is observed that in the absence of the photo catalyst, there was only 5% degradation of the dye during the same period of irradiation (Fig. 10a). This indicates that as prepared ZnS is an effective photo catalyst for the degradation of RhB. Fig. 10b shows the percentage of degradation of RhB using ZnS catalyst. About 87% of RhB is degraded during 150 min of irradiation for ZSH1 sample. And 73%, 61%, 53% and 47% of RhB is degraded with ZSH2, ZSH3, ZSH8 and ZSH9 samples. This suggests that ZSH1 act as better photo catalyst than other ZnS catalysts. The photo-catalytic degradation kinetics of RhB is analysed and shown in Fig. 10c. The reaction assumed to follow pseudo first order kinetic, which is given in the following equation,

$$\ln\left(\frac{C}{C_0}\right) = -kt \tag{4}$$

where, C_0 is the initial concentration of RhB and C is the concentration at time t. The plot of ln C/Co versus time is a straight line with a slope k, known as rate constant. The values of the rate constants are given in Table 2. It can be seen from Table 2 that the highest k is observed with ZSH1 i.e., 0.0113 min^{-1}. The k for ZSH2, ZSH3, ZSH8 and ZSH9 are calculated to be 0.0083, 0.0058, 0.0049 and 0.0041 min^{-1}, respectively. This indicates that ZSH1 has shown better catalytic activity than the remaining ZnS samples. This may be due to smaller particle size of ZSH1, resulted to the larger surface area than the remaining ZnS samples. Dong et al. [20] also reported the photo catalytic activity of L-Histidine assisted ZnS microsphere and the efficient photo catalytic activity was found to be greater for the ZnS microsphere having smaller particle size.

The k for degradation of RhB with ZnS and carbon quantum dot ZnS catalysts are reported to be 0.0054 min^{-1} and 0.011 min^{-1} [55]. Therefore our ZnS samples shows good catalytic activity.

The stability of the photo catalyst is important for industrial use. The reusability test for ZSH1 and ZSH9 are carried out, which is shown in Fig. 10d. In both catalysts, the degradation efficiency remain constant up to third cycles. Hence the catalysts are found to be stable upto third cycles, which suggests the good stability of the catalysts.

The degradation of RhB occurs either by *N*-de methylation or the destruction of the conjugated structure [56]. The decrease in the absorption of RhB solution at 554 nm attributes to the destruction of the conjugated structure. The absorption band of RhB blue shifted with the irradiation suggests the formation of de-ethylated RhB molecule [57,58]. In this present studies, since there is a blue shift in absorption maxima with time of irradiation, it infers that the degradation of RhB is mainly due to the *N*-demethylation process.

The degradation mechanism can be explained as follows:

When ZnS absorbs photons of energy higher than or equal to its band gap, electrons are generated to conduction band and holes to the valence band. The photo generated electrons react with dissolved O_2 molecules producing superoxide anion ($^{\bullet}O_2^-$) radicals, while holes react with H_2O and produce hydroxyl ($^{\bullet}OH$) radicals. The $^{\bullet}O_2^-$ and OH radicals causes the degradation of the RhB dye. These reactions can be schematically illustrated in Scheme 1.

It has been reported that the blue-shift of the absorption band caused by de-ethylation of RhB is due to the attack by one of the active oxygen species on the *N*-ethyl group [59]. Therefore the degradation of the RhB dye in the present studies might have occurred predominantly through Eq. (4).

$$ZnS \xrightarrow{h\upsilon} e^- (CB) + h^+ (VB) \quad \text{.....(1)}$$

$$e^- + O_2 \longrightarrow \cdot O_2^- \quad \text{.....(2)}$$

$$h^+ + OH^- \longrightarrow \cdot OH \quad \text{.....(3)}$$

$$\cdot O_2^- + \text{RhB dye} \longrightarrow \text{Degradation of RhB} \quad \text{.....(4)}$$

$$\cdot OH + \text{RhB dye} \longrightarrow \text{Degradation of RhB} \quad \text{.....(5)}$$

Scheme 1. The reaction mechanism of photocatalytic degradation of RhB.

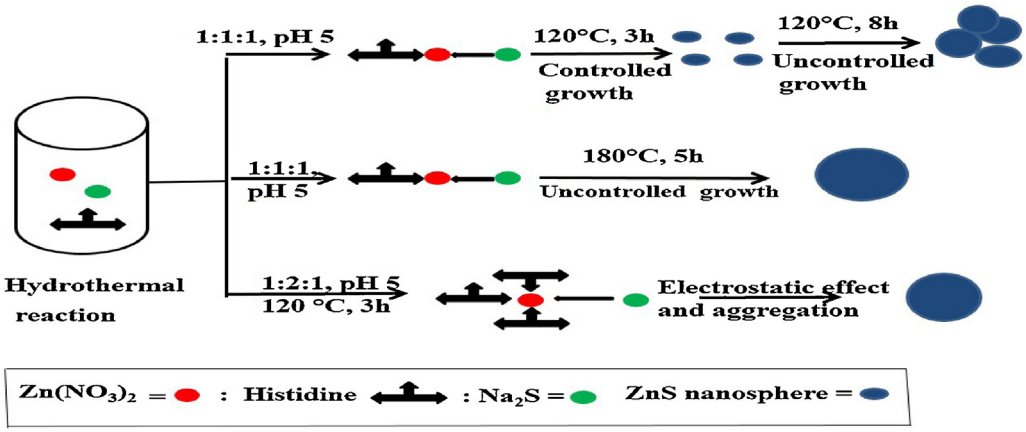

Scheme 2. Mechanism for the formation of ZnS nanosphere.

4. Mechanism for the formation of ZnS nanosphere

Crystal growth process consists of three steps: nucleation, dissolution and recrystallization process [60]. With increase in reaction temperature and time, the crystal growth rate is accelerated. The rate of nucleation and growth is depending on the temperature and time. The formation of ZnS nanosphere is illustrated in Scheme 2 At 120 °C and 3 h duration, the ZnS was found to uniformly disperse with particle size of 5 nm diameter range. When the duration of time and reaction temperature was increased the smaller nanoparticles are quickly aggregated resulting into the formation of bigger particle size. Not only the particle size increases but also the morphology of the particle changes. The presence of high L-Histidine concentration influences more electrostatic effect which resulted into the increase in the aggregation process leading into bigger particle size.

5. Conclusion

In conclusion, ZnS nanosphere was prepared by hydrothermal method using L-Histidine as capping agent. The average particle size of 5 nm was obtained with the reaction parameter at 120 °C temperature and duration 3 h. Increase in reaction temperature and time, the particle size increases as observed from XRD and TEM images. PL depends on the various reaction parameters. A reducing trend in the emission intensity is noticed from PL spectra with increase in reaction time and temperature. This ZnS act as a good photo catalyst and observed 87% of RhB degradation in 150 min with ZnS sample having particle size of 5 nm. This study demonstrates the role of reaction parameters to tune the desire ZnS nanosphere and simple light source, sunlight, was used to see the photo catalytic activity of ZnS.

Acknowledgements

Authors are sincerely acknowledged Department of Science & Technology, Government of India for financial support vide reference no SR/WOS-A/CS-120/2013 under Women Scientist Scheme to carry out this work. Prof P.T Manoharan, Department of Chemistry, IIT Madras, India is thankful for his kind support. Mrs S.G. Chatterjee, CMSNT, SMIT, India and Ms Laden Sherpa, Department of Physics, Sikkim University, India are acknowledged for their help in IR and PL measurements.

Appendix A. Supplementary data

Supplementary data associated with this article can be found, in the online version, at http://dx.doi.org/10.1016/j.apsusc.2016.05.045.

References

[1] T.I. Chanu, T. Muthukumar, P.T. Manoharan, Fuel mediated solution combustion synthesis of ZnO supported gold clusters and nanoparticles and their catalytic activity and in vitro cytotoxicity, Phys. Chem. Chem. Phys. 16 (2014) 23686–23698.
[2] S.K. Nandi, S. Chatterjee, S.K. Samanta, G.K. Dalapati, P.K. Bose, S. Varma, S. Patil, C.K. Maiti, Electrical properties of Ta_2O_5 films deposited on ZnO, Bull. Mater. Sci. 26 (2003) 365–369.
[3] X. Fang, T. Zhai, U.K. Gautam, L. Li, L. Wu, Y. Bando, D. Golberg, ZnS nanostructures: from synthesis to applications, Prog. Mater. Sci. 56 (2011) 175–287.
[4] N. Üzar, M.Ç. Arikan, Synthesis and investigation of optical properties of ZnS nanostructures, Bull. Mater. Sci. 34 (2011) 287–292.
[5] T.W. Sung, Y.L. Lo, Highly sensitive and selective sensor based on silica-coated CdSe/ZnS nanoparticles for Cu^{2+} ion detection, Sens. Actuators B 165 (2012) 119–125.
[6] Y.C. Chen, C.H. Wang, H.Y. Lin, B.H. Li, W.T. Chen, C.P. Liu, Growth of Ga-doped ZnS nanowires constructed by self-assembled hexagonal platelets with excellent photocatalytic properties, Nanotechnology 45 (2010) 455604.

[7] K. Manzoor, S. Johny, D. Thomas, S. Setua, D. Menon, S. Nair, Bio-conjugated luminescent quantum dots of doped ZnS: a cyto-friendly system for targeted cancer imaging, Nanotechnology 6 (2009) 065102.
[8] C.L. Cowles, X. Zhu, Sensitive detection of cardiac biomarker using ZnS nanoparticles as novel signal transducers, Biosens. Bioelectron. 30 (2011) 342–346.
[9] Z. Wang, L.L. Daemen, Y. Zhao, C.S. Zha, R.T. Downs, X. Wang, Z.L. Wang, R.J. Hemley, Morphology-tuned wurtzite-type ZnS nanobelts, Nat. Mater. 4 (2005) 922.
[10] X. Li, X. Wang, Q. Xiong, P.C. Eklund, Mechanical properties of ZnS nanobelts, Nano Lett. 5 (2005) 10.
[11] G. Murugadoss, Synthesis and photoluminescence properties of zinc sulfide nanoparticles doped with copper using effective surfactants, Particuology 11 (2013) 566–573.
[12] J.S.M. Cloy, B.G. Potter, Photoluminescence in chemical vapor deposited. ZnS: insight into electronic defects, Opt. Mater. Express 3 (2013) 1275.
[13] J.G. Zhao, H.H. Zhang, Hydrothermal synthesis and characterization of ZnS hierarchical microspheres, Super Lattices. Microstruct. 51 (2012) 663–667.
[14] S. Li, Z. Wu, W. Li, Y. Liu, R. Zhuo, D. Yan, W. Juna, P. Yanab, One-pot synthesis of ZnS hollow spheres via a low temperature, template-free hydrothermal route, CrystEngComm 15 (2013) 1571.
[15] G.O. Siqueira, T. Matencio, H.V. Silva, Y.G. Souza, J.D. Ardisson, G.M. Limaa, A.O. Porto, Temperature and time dependence on ZnS microstructure and phases obtained through hydrothermal decomposition of diethyldithiocarbamate complexes, Phys. Chem. Chem. Phys. 15 (2013) 6796.
[16] L. Chen, C. Wang, Q. Li, S. Yang, L. Hou, S. Chen, In situ synthesis of transparent fluorescent ZnS–polymer nanocomposite hybrids through catalytic chain transfer polymerization technique, J. Mater. Sci. 44 (2009) 3413–3419.
[17] S. Kar, C. Patel, S. Santra, Direct room temperature synthesis of valence state engineered ultra-small ceria nanoparticles: investigation on the role of ethylenediamine as a capping agent, J. Phys. Chem. C 113 (2009) 4862–4867.
[18] G. Chen, Y. Xie, R. Peltier, H. Lei, P. Wang, J. Chen, Y. Hu, F. Wang, X. Yao, H. Sun, Peptide-decorated gold nanoparticles as functional nano-capping agent of mesoporous silica container for targeting drug delivery, ACS, Appl. Mater. Interfaces 8 (18) (2016) 11204–11209.
[19] Q. Wu, X. Chen, P. Zhang, Y. Han, X. Chen, Y. Yan, S. Li, Amino acid-assisted synthesis of ZnO hierarchical architectures and their novel photocatalytic activities, Cryst. Growth Des. 8 (2008) 3011.
[20] F. Dong, Y. Guon, J. Zhang, Y. Li, L. Yangn, Q. Fang, H. Fang, K. Jiang, Size-controllable hydrothermal synthesis of ZnS nanospheres and the application in photocatalytic degradation of organic dyes, Mater. Lett. 97 (2013) 59–63.
[21] Y. Tao, Y. Xu, J.P.H. Gu, C. Qin, P. Zhou, Glycine assisted synthesis of flower-like TiO_2 hierarchical spheres and its application in photocatalysis, Mater. Sci. Eng. B 177 (2012) 1664–1671.
[22] D.A. Reddy, D.H. Kim, S.J. Rhee, B.W. Lee, C. Liu, Tunable blue-green-emitting wurtzite ZnS:Mg nanosheet-assembled hierarchical spheres for near-UV white LEDs, Nanoscale Res. Lett. 9 (2014) 20.
[23] A.A. Khosravi, M. Kundu, L. Jatwa, S.K. Deshpande, U.A. Bhagwat, Green luminescence from copper doped zinc sulphide quantum particles, Appl. Phys. Lett. 67 (1995) 2702.
[24] R. Kripal, A.K. Gupta, S.K. Mishra, R.K. Srivastava, A.C. Pandey, S.G. Prakash, Photoluminescence and photoconductivity of ZnS:Mn^{2+} nanoparticles synthesized via co-precipitation method, Spectrochim. Acta A 76 (2010) 523–530.
[25] H. Li, W.Y. Shih, W.H. Shih, Highly photoluminescent and stable aqueous ZnS quantum dots, Ind. Eng. Chem. Res. 49 (2010) 578–582.
[26] X. Zeng, S. Yan, J. Cui, H. Liu, J. Dong, W. Xia, M. Zhou, H. Chen, Size- and morphology-dependent optical properties of ZnS:Al one-dimensional structures, J. Nanopart. Res. 17 (2015) 188.
[27] B.Y. Geng, X.W. Liu, Q.B. Du, X.W. Wei, L.D. Zhang, Structure and optical properties of periodically twinned ZnS nanowires, Appl. Phys. Lett. 88 (2006) 163104.
[28] Y. Zhang, C. Pan, Y. Zhang, W. He, Self-template hydrothermal synthesis ZnS microspheres, Cryst. Res. Technol. 46 (2011) 718–722.
[29] C. Ye, X. Fang, M. Wang, L. Zhang, Temperature-dependent photoluminescence from elemental sulfur species on ZnS nanobelts, J. Appl. Phys. 99 (2006) 063504.
[30] V.P. Devarajan, D. Nataraj, T. Pazhanivel, K. Senthil, M. Seol, K. Yong, J. Hermannsdorfere, R. Kempee, Molecular conformation dependent emission behaviour (blue, red and white light emissions) of all-*trans*-β-carotene-ZnS quantum dot hybrid nanostructures, J. Mater. Chem. 22 (2012) 18454.
[31] H. Yang, C. Huang, X. Su, A. Tang, Microwave-assisted synthesis and luminescent properties of pure and doped ZnS nanoparticles, J. Alloy Compd. 402 (2005) 274–277.
[32] J. Zhang, Effect of effective mass and spontaneous polarization on photocatalytic activity of wurtzite and zinc-blende ZnS, APL Mater. 3 (2015) 104404.
[33] J. Zhang, J. Yu, Y. Zhang, Q. Li, J.R. Gong, Visible light photocatalytic H_2-production activity of CuS/ZnS porous nanosheets based on photoinduced interfacial charge transfer, Nano Lett. 11 (2011) 4774–4779.
[34] R.J.V. Michael, J. Theerthagiri, J. Madhavan, M.J. Umapathy, P.T. Manoharan, Cu_2S-incorporated ZnS nanocomposites for photocatalytic hydrogen evolution, RSC Adv. 5 (2015) 30175.
[35] N. Soltani, E. Saion, W.M.M. Yunus, M. Erfani, M. Navasery, G. Bahmanrokh, K. Rezaee, Enhancement of visible light photocatalytic activity of ZnS and CdS nanoparticles based on organic and inorganic coating, Appl. Surf. Sci. 290 (2014) 440–447.
[36] D.A. Reddy, R. Ma, M.Y. Choi, T.K. Kim, Reduced graphene oxide wrapped ZnS-Ag_2S ternary composites synthesized via hydrothermal method: applications in photocatalyst degradation of organic pollutants, Appl. Surf. Sci 324 (2015) 725–735.
[37] Y. Lixiong, W. Dan, H. Jianfeng, C. Liyun, O. Haibo, Y. Xiang, Morphology-controllable synthesis and enhanced photocatalytic activity of ZnS nanoparticles, J. Alloy Compd. 664 (2016) 476–480.
[38] Z. Han, X. Zheng, F. Hu, F. Qu, A. Umar, X. Wu, Facile synthesis of hollow ZnS nanospheres for environmental remediation, Mater. Lett. 160 (2015) 271–274.
[39] Z. Bin, C. Xiaohua, T. Qianxiang, C. Chuansheng, H. Aiping, Ordered mesoporous necklace-like ZnS on graphene for use as a high performance photocatalyst, Appl. Surf. Sci. 308 (2014) 321–327.
[40] J. Zhang, S. Liu, J. Yu, M. Jaroniec, A simple cation exchange approach to Bi-doped ZnS hollow spheres with enhanced UV and visible-light photocatalytic H_2-production activity, J. Mater. Chem. 21 (2011) 14655–14662.
[41] A.A.P. Mansur, H.S. Mansur, F.P. Ramanery, L.C. Oliveira, P.P. Souza, Green colloidal ZnS quantum dots/chitosan nano-photocatalysts for advanced oxidation processes: study of the photodegradation of organic dye pollutants, Appl. Catal B—Environ. 158 (2014) 269–279.
[42] L.M. Devi, D.P.S. Negi, Effect of starting pH and stabilizer/metal ion ratio on the photocatalytic activity of ZnS nanoparticles, Mater. Chem. Phys. 141 (2013) 797.
[43] M.H. Ullah, I. Kim, C.S. Ha, pH selective synthesis of ZnS nanocrystals and their growth and photoluminescence, Mater. Lett 61 (2007) 4267–4271.
[44] W.T. Chen, Y.J. Hsu, L-Cysteine assisted growth of core-satellite ZnS-Au nanoassemblies with high photocatalytic efficiency, Langmuir 26 (2010) 5918–5925.
[45] Z.H. Ibupoto, K. Khun, X. Liu, M. Willander, Hydrothermal synthesis of nanoclusters of ZnS comprised on nanowires, Nanomaterials 3 (2013) 564–571.
[46] G. Murugadoss, R. Jayavel, M.R. Kumar, R. Thangamuthu, Synthesis, optical, photocatalytic, and electrochemical studies on Ag_2S/ZnS and ZnS/Ag_2S nanocomposites, Appl. Nanosci. 6 (2016) 503–510.
[47] N. Soltani, A. Dehzangi, A. Kharazmi, E. Saion, W.M.M. Yunus, B.Y. Majlis, M.R. Zare, E. Gharibshahi, N. Khalilzadeh, Structural, optical and electrical properties of ZnS nanoparticles affecting by organic coating, Chalcogenide Lett. 11 (2014) 79–90.
[48] X. Wang, J. Shi, Z. Feng, M. Li, C Li, Visible emission characteristics from different defects of ZnS nanocrystals, Phys. Chem. Chem. Phys. 13 (2011) 4715–4723.
[49] H.Y. Lu, S.Y. Chu, S.S. Tan, The characteristics of low-temperature-synthesized ZnS and ZnO nanoparticles, J. Cryst. Growth 269 (2004) 385–391.
[50] R.J. Sundberg, R.B. Martin, Interactions of Histidine and other imidazole derivatives with transition metal ions in chemical and biological systems, Chem. Rev. 74 (1974) 4472.
[51] M. Hafeez, S. Rehman, U. Manzoor, M.A. Khan, A.S. Bhatti, Catalyst driven optical properties of the self-assembled ZnS nanostructures, Phys. Chem. Chem. Phys. 15 (2013) 9726.
[52] D. Denzler, M. Olschewski, K. Sattler, Luminescence studies of localized gap states in colloidal ZnS nanocrystals, J. Appl. Phys. 84 (1998) 2841–2845.
[53] A.K. Kole, C.S. Tiwary, P. Kumbhakar, Morphology controlled synthesis of wurtzite ZnS nanostructures through simple hydrothermal method and observation of white light emission from ZnO obtained by annealing the synthesized ZnS nanostructures, J. Mater. Chem. C 2 (2014) 4338.
[54] C. Ye, X. Fang, G. Li, L. Zhang, Origin of the green photoluminescence from zinc sulfide nanobelts, Appl. Phys. Lett. 85 (2004) 035.
[55] F. Ming, J. Hong, X. Xu, Z. Wan, Dandelion-like ZnS/carbon quantum dots hybrid materials with enhanced photocatalytic activity toward organic pollutants, RSC Adv. 6 (2016) 31551–31558.
[56] C. Chen, X. Li, W. Ma, J. Zhao, H. Hidaka, N. Serpone, Effect of transition metal ions on the TiO_2-assisted photodegradation of dyes under visible irradiation: a probe for the interfacial electron transfer process and reaction mechanism, J. Phys. Chem. B 106 (2002) 318.
[57] Y. Cui, Z. Ding, P. Liu, M. Antonietti, X. Fu, X. Wang, Metal-free activation of H_2O_2 by g-C_3N_4 under visible light irradiation for the degradation of organic pollutants, Phys. Chem. Chem. Phys. 14 (2012) 1455–1462.
[58] J. Li, X. Zhang, Z. Ai, F. Jia, L. Zhang, J. Lin, Efficient visible light degradation of rhodamine B by a photo-electrochemical process based on a Bi_2WO_6 nanoplate film electrode, J. Phys. Chem. C 111 (2007) 6832–6836.
[59] Z. Shen, G. Chen, Y. Yu, Q. Wang, C. Zhou, L. Hao, Y. Li, L. He, R. Mu, Sonochemistry synthesis of nanocrystals embedded in a MoO_3–CdS core-shell photocatalyst with enhanced hydrogen production and photodegradation, J. Mater. Chem. 22 (2012) 19646–19651.
[60] N.T.K. Thanh, N. Maclean, S. Mahiddine, Mechanisms of nucleation and growth of nanoparticles in solution, Chem. Rev. 114 (2014) 7610–7630.